Spectral Gap Superposition States

Davide Cugini,[1, *] Francesco Ghisoni,[1, †] Angela Rosy Morgillo,[1, ‡] and Francesco Scala[1, §]

[1]*Dipartimento di Fisica, Università degli Studi di Pavia, via A. Bassi 6, 27100 Pavia (Italy)*
(Dated: February 28, 2024)

This work introduces a novel NISQ-friendly procedure for estimating spectral gaps in quantum systems. By leveraging Adiabatic Thermalization, we are able to create the Spectral Gap Superposition state, a newly defined quantum state exhibiting observable fluctuations in time that allow for the accurate estimation of any energy gap. Our method is tested by estimating the energy gap between the ground and the first excited state for the 1D and 2D Ising model, the Hydrogen molecule H_2 and Helium molecule He_2. Despite limiting our circuit design to have at most 40 Trotter steps, our numerical experiments of both noiseless and noisy devices for the presented systems give relative errors in the order of 10^{-2} and 10^{-1}. Further experiments on the IonQ Aria device lead to spectral gap estimations with a relative error of 10^{-2} for a 4-site Ising chain, demonstrating the validity of the procedure for NISQ devices and charting a path towards a new way of calculating energy gaps.

I. INTRODUCTION

The estimation of the spectral gap, defined as the energy difference between the ground state and the first excited state of a quantum system, is fundamental in both condensed matter physics and quantum chemistry. Its numerical calculation on classical computers has two major hurdles: the sign problem for fermionic systems [1] and the exponentially increasing computational cost with the system size. The advent of Quantum Computation has given researchers tools to potentially overcome these fundamental issues. Currently, we are in the so-called Noisy Intermediate-Scale Quantum (NISQ) era [2], in which devices have limited number of noisy qubits. In fact, researchers have sought ways to employ these devices to come up with estimation techniques for the energy gap. Some examples include: imaginary time propagation [3], and robust phase estimation [4].

In this work, we introduce a novel approach for estimating the energy gaps in quantum systems. We define the Spectral Gap Superposition (SGS) state as

$$|SGS(i,j)\rangle = \frac{1}{\sqrt{2}} \left(|\Omega_i\rangle + |\Omega_j\rangle \right), \qquad (1)$$

where $|\Omega_i\rangle$ and $|\Omega_j\rangle$ respectively are the i-th and j-th eigenstates of the system Hamiltonian H. Although the two eigenstates are not known analytically, they can be prepared on a quantum computer through Adiabatic Thermalization (AT) [5] if the adiabatic theorem conditions hold [6]. In this regime we show that it is possible to utilize the time fluctuations of observables evaluated on the SGS state to obtain an estimate of the energy gap $\Delta E_{j,i}$ between the energies of $|\Omega_j\rangle$ and $|\Omega_i\rangle$.

_____

* davide.cugini01@universitadipavia.it
† francesco.ghisoni01@universitadipavia.it
‡ angelarosy.morgillo01@universitadipavia.it
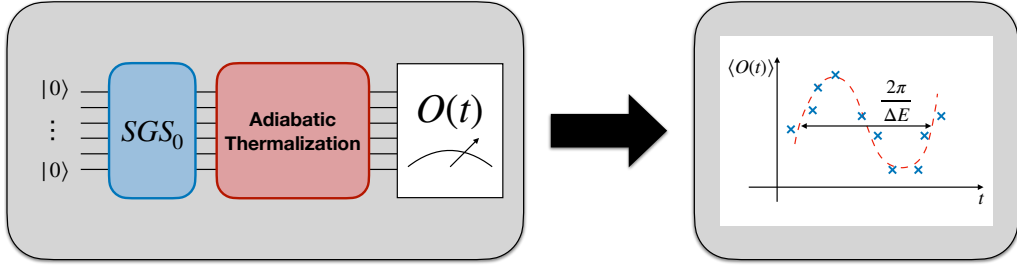§ francesco.scala01@universitadipavia.it

This report is organized as follows. In Section II we present our procedure, showing its derivation and underlying principles. In Section III we report the numerical results of our method applied for the spectral gap estimation of the Ising model, on a classical computer simulator, followed by the outcomes obtained with the real hardware IonQ Aria. It follows a detailed description of the spectral gap estimation for the H_2 and He_2 molecules run on a classical computer simulator. Finally, in Section IV, we provide a comprehensive summary and draw conclusions from our findings.

II. SPECTRAL GAP ESTIMATION

Let $O(t)$ be a time dependent operator of type

$$O(t) = e^{iHt} O e^{-iHt} \qquad (2)$$

where H is the Hamiltonian of a physical system. The expectation value of the observable $O(t)$ calculated on the SGS state (1) is

$$\langle O(t)\rangle = \frac{1}{2} \left(\langle\Omega_i| O |\Omega_i\rangle + \langle\Omega_j| O |\Omega_j\rangle \right) + \\ + \rho \cos\left(\Delta E_{ji} t + \theta\right), \qquad (3)$$

where $\rho > 0$ and $\theta \in [0, 2\pi)$ are the polar coordinates of the complex number $\langle\Omega_j| O |\Omega_i\rangle$. From Equation (3) one could obtain an estimate of the energy gap by fitting the $\langle O(t)\rangle$ function over the time variable.

To obtain $\langle O(t)\rangle$ one should (i) prepare the SGS state on a quantum computer, (ii) implement the time evolution e^{-iHt} as a quantum circuit and (iii) compute the expectation value of an operator O (see Figure 1). The state preparation can be performed via the AT. This allows to evolve the n-th eigenstate $|\omega_n\rangle$ of an auxiliary Hamiltonian H_0 into the n-th eigenstate of H through the evolution operator U_τ, i.e.

$$\lim_{\tau \to \infty} U_\tau |\omega_n\rangle = |\Omega_n\rangle, \qquad (4)$$

FIG. 1: Schematic representation of the proposed methodology. Initially, a quantum circuit generates a Spectral Gap Superposition (SGS$_0$) state of two eigenstates of the auxiliary Hamiltonian H_0. Through Adiabatic Thermalization this state is evolved to the SGS state of the system Hamiltonian H. Sequential measurements of the chosen observable $O(t)$ at different time steps are recorded. Finally a fitting process is used to determine the spectral gap. The obtained value is compared to the benchmark spectral gap.

where $\tau > 0$ represents the thermalization time. This guarantees that if one is able to prepare the superposition

$$|SGS_0\rangle = \frac{1}{\sqrt{2}}\left(|\omega_0\rangle + |\omega_1\rangle\right) \qquad (5)$$

then it is enough to thermalize it to get

$$\lim_{\tau \to \infty} U_\tau |SGS_0\rangle = |SGS\rangle. \qquad (6)$$

The AT evolution, like the time evolution operator of step (ii), can be implemented through the *Trotter-Suzuki method* [7].

It is important to note that, as long as $\rho > 0$, any observable O can be used in Equation (3) to estimate the energy gap. *A priori* knowledge of the system should be used to find the observable that maximizes ρ, since this facilitates the fitting process. Observe that our procedure allows, in principle, to estimate the energy gap between two arbitrary eigenstates of H. Moreover, this is done without separately calculating the two energy eigenvalues, keeping the overall computational cost as low as possible.

III. NUMERICAL RESULTS

In this section, we present the numerical tests with the developed procedure. In the perspective of implementing the numerical studies on a Quantum device, we restrict the circuits to be composed of 40 Trotter steps. From now on we use the following notation for the 2×2 identity operator and the Pauli matrices

$$\sigma^0 = I, \quad \sigma^1 = \sigma^x, \quad \sigma^2 = \sigma^y, \quad \sigma^3 = \sigma^z. \qquad (7)$$

A. Ising model

Our first test case is the L-sites Ising model [8] with Periodic Boundary Conditions (PBC), described by the Hamiltonian

$$H = -\frac{J_1}{2} \sum_{\langle ij \rangle} \sigma_i^1 \sigma_j^1 - \frac{h_3}{2} \sum_i \sigma_i^3, \qquad (8)$$

where σ_i is a Pauli matrix acting on site i and the $\langle \cdot \cdot \rangle$ symbol restricts the sum over the nearest neighbors. In what follows, we restrict to the case of positive coupling constants $h_3, J_1 \geq 0$. To find the spectral gap we need to prepare the SGS state

$$|SGS(0,1)\rangle = \frac{1}{\sqrt{2}}(|\Omega_0\rangle + |\Omega_1\rangle). \qquad (9)$$

For this scope we consider the auxiliary Hamiltonian

$$H_0 = -\frac{J_1}{2} \sum_{\langle ij \rangle} \sigma_i^1 \sigma_j^1. \qquad (10)$$

The ground state of H_0 space is degenerate with dimension 2 and is spanned by $|+\rangle^{\otimes L}$ and $|-\rangle^{\otimes L}$, which are defined as:

$$|\pm\rangle \equiv \frac{1}{\sqrt{2}}\left(|0\rangle \pm |1\rangle\right). \qquad (11)$$

Preparing $|SGS_0\rangle$ requires the right linear combination of $|+\rangle^{\otimes L}$ and $|-\rangle^{\otimes L}$. From symmetry considerations, which are reported in Appendix B, we find

$$|SGS_0(0,1)\rangle = |+\rangle^{\otimes L}. \qquad (12)$$

All experiments conducted for the Ising model, both in 1D and 2D, use the observable

$$O = \sigma^3 \otimes \left(\sigma^0\right)^{\otimes (L-1)}. \qquad (13)$$

Numerical experiments demonstrate that this observable maximizes ρ in Equation (3) for any Ising chain (1D case) and square lattice (2D case). The full investigation can be found in in Appendix C.

The presented experiments are a 4 site Ising chain with PBC. It is important to note that the circuit depth per

Trotter step needed to simulate Ising is independent of the number of sites L. In particular, all experiments involving the 4-site Ising chain, including noiseless, noisy and real hardware, have a maximum depth of 80 2-qubit gates once composed with IonQ native gates. More information can be seen in Appendix F.

The 40 Trotter steps are divided in 15 thermalization steps and 25 time evolution steps. We choose the 25 times t for the evaluation of $O(t)$ to be Chebyshev-distributed to facilitate the fitting process [9] (see Appendix D). Each circuit is simulated on a classical computer with 8192 shots. We take the intrinsic error of the quantum state measurement into account as described in Appendix E. All simulated results are compared to a numerical benchmark which is calculated using direct diagonalization of the Hamiltonian H.

The numerical results for the 4-site Ising chain, presented in Figure 2, show an excellent agreement between the numerical benchmark and the noiseless estimated spectral gap for $L = 4$. The graph illustrates the spectral gap dependence on the parameter h_3/J_1. The relative error between the noiseless numerical results and the benchmark is in the order of 10^{-2}.

The infrared and adiabatic limits are regimes where our approach becomes unstable, within the imposed number of Trotter steps[1]. In the infrared limit, the $O(t)$ frequency tends to zero and its estimation would require a huge amount of time steps for the time evolution. The adiabatic limit, instead, requires long thermalization time for a high fidelity state preparation.

Remarkably, our approach exhibits strong resilience when subjected to the noise model inspired by IonQ Aria 1. Specifically, the impact of thermal relaxation and readout are minimal due to the extended T_1 and T_2 parameters and small readout error, while the biggest error contribution is due to 2-qubit gate average fidelities (see Appendix F for more details on the hardware noise model). The average relative error between the numerical and the estimated gap has been determined to be of order 10^{-1}. Moreover, further investigation revealed that the procedure has also strong resilience to reduced number of shots (see Appendix F).

Analogous results are obtained for the 4-site Ising lattice and are reported in Appendix G.

IonQ Aria Device

The final test for the SGS procedure on a 4 site Ising chain is the IonQ Aria 1 device. Due to resource limitations, the conducted experiments used slightly different specs compared to the noiseless and noisy experiments. Firstly, the energy gap for only 3 different h_3/J_1 values is
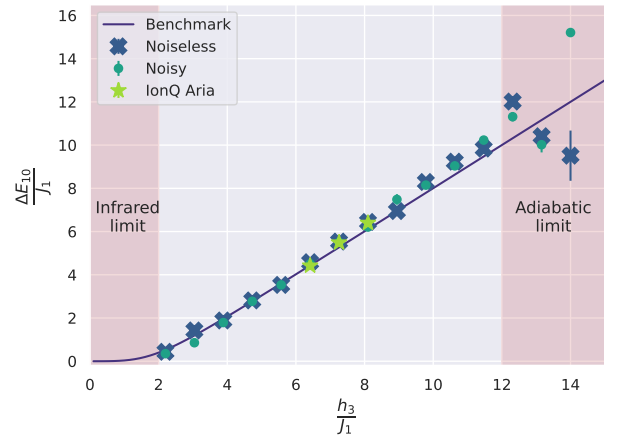
---

[1] One can always try to balance the reduced number of Trotter steps with longer time steps, but at a certain point, the Trotter-Suzuki approximation would no longer hold.

FIG. 2: Spectral gap as a function of h_3/J_1 for a $L = 4$ Ising chain with PBC. The plot includes simulations on a classical computer, showing both noiseless and noisy results, and experiments on IonQ Aria 1. Our approach demonstrates optimal agreement with the benchmark values, highlighting the robustness of our method for execution on NISQ hardware. The adiabatic and infrared limits are regions where the circuit depth used is insufficient. Error bars represent a single standard deviation computed from the fit.

found. These values are selected since they are far from both the infrared and adiabatic limits. Secondly, only a subset of 10 times t of the initial 25, are employed for the fitting of $O(t)$. Finally, 2500 shots (with error mitigation) are used instead of 8192 employed in the numerical simulations (without error mitigation).

The results, shown in Figure 2, reveal agreement between the noiseless simulation, the noisy simulation, and the IonQ Aria device. This witnesses the robustness of our approach to noise (both simulated and real). It is worth mentioning that the IonQ Aria device comes with integrated error mitigation for a minimum number of 2500 shots, which likely contributed to the consistent results obtained in our study (more details in Appendix F). Moreover, thanks to noise mitigation results on real hardware are actually better than the ones obtained with noisy simulations as they have a bigger ρ (see Appendix F).

B. H$_2$ and He$_2$ molecules

In this section, we present the results of our spectral gap estimation applied to the H$_2$ and He$_2$ molecules.

In general, a molecular Hamiltonian $\mathcal{H}$ is expressed as [10]

$$\mathcal{H} = \sum_{pq} h_{pq} c_p^\dagger c_q + \frac{1}{2} \sum_{pqrs} h_{pqrs} c_p^\dagger c_q^\dagger c_r c_s. \qquad (14)$$

The coefficients h_{pq} and h_{pqrs}, specific to each molecu-

lar system, respectively parametrize the one-body and two-body electron-electron interactions. The operators c_p and $c_p^\dagger$ represent the fermionic annihilation and creation operators acting on an electron in the atomic orbital p. The physical Hamiltonian (14) can be mapped on N-qubits via the Jordan-Wigner transformation [11], given by the following equation:

$$H = \Sigma_{i_1,...,i_L} \left[a_{i_1,...,i_L} \bigotimes_{j=1}^{L} \sigma^{i_j} \right], \quad i_j \in \{0,1,2,3\} .$$

(15)

Given the objective to create the $|SGS(0,1)\rangle$ state, we take the auxiliary Hamiltonian to be the diagonal of H

$$H_0 = \text{diag}(H).$$

(16)

Since H_0 is diagonal, the eigenstates will be elements of the computational basis, making them easy to prepare on a quantum computer. In addition, one can immediately associate each eigenstate to its eigenvalue.

The state $|SGS_0(0,1)\rangle$ is prepared by selecting a superposition comprising any ground state $|\omega_0\rangle$ and first excited state $|\omega_1\rangle$ of H_0. Despite the procedure returning accurate estimates for a wide range of bond lengths, as seen in Figure 3, we believe that symmetry considerations would aid the state preparation.

The choice of operators for small molecules is fully discussed in Appendix C. These considerations result in an operator O of the form

$$O = \bigotimes_{j=1}^{L} \sigma_j^{i_j} \quad i_j \in \{0,1\}$$

(17)

which is a tensor product of identities and σ^1 matrices such that:

$$|\langle \omega_1 | O | \omega_0 \rangle| = 1$$

(18)

where $|\omega_i\rangle$ are the ground and excited state of the auxiliary Hamiltonian.

The experiments for the molecules involve the calculation of the energy gap as a function of the bond length for H_2 and He_2. For both experiments 40 Trotter steps are used, using 5 thermalization steps and 35 time evolution steps. The H_2 Hamiltonian requires 4 qubits, while the He_2 Hamiltonian requires 8 qubits.

The results from the noiseless simulations of a H_2 molecule can be seen in Figure 3a, while those for He_2 are in Figure 3b. The noiseless simulation results demonstrate excellent agreement with the benchmark values, exception made for a couple of points for H_2 possibly due to the choice of the observable, as discussed above.

IV. DISCUSSION

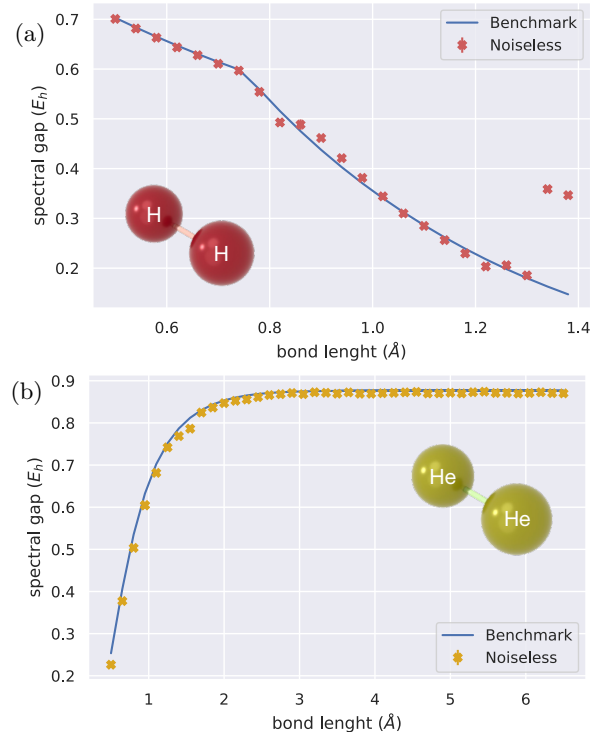We have developed a novel NISQ-friendly procedure to perform energy gap estimations for a wide range of

FIG. 3: (a) The plot illustrates the spectral gap of the H_2 molecule as a function of the bond length. The noiseless simulation results demonstrate excellent agreement with the benchmark values. (b) The plot illustrates the spectral gap of the He_2 molecule as a function of the bond length. Error bars represent a single standard deviation computed from the fit.

Hamiltonians. Although a procedure that implements time evolution to obtain information on spectral gaps has been previously attempted [12], our improved method is able to specifically estimate any desired energy gap by preparing a tailored Spectral Gap Superposition state exploiting the Adiabatic Thermalization method. We demonstrated the capabilities of our spectral gap estimation procedure on the Ising model, both 1D and 2D, as well as small molecular systems, H_2 and He_2. Experiments were conducted using at most 40 Trotter steps to use circuit depths comparable with ones available with NISQ devices. Our procedure was able to find energy gaps with relative errors of the order of 10^{-2} for noiseless simulations. The experiments demonstrate the procedure holds surprisingly well when reducing the number of shots to 100. Furthermore, we were able to accurately model the noise of the IonQ Aria 1 device. This led us to launch experiments on the IonQ Aria 1 device and successfully estimate the energy gap of a 4-site Ising chain with a relative error of the order of 10^{-2}. Given the current pace of development in quantum computing hardware, we believe this procedure could be used for energy gap estimation of bigger molecules and condensed matter systems in the near term. In addition, it is worth not-

ing that any major breakthrough in either the accuracy or the computational cost of adiabatic thermalization, which is an active field of research, will also drastically improve the presented energy gap estimation procedure. This work opens up the way to effective quantum computation on NISQ devices for both academic and industrial endeavors in the realm of Condensed Matter Physics and Quantum Chemistry.

V. APPENDIX

Appendix A: Adiabatic Thermalization

Let $H(t)$ be the time dependent Hamiltonian

$$H(t) = \left(1 - \frac{t}{\tau}\right) H_0 + \left(\frac{t}{\tau}\right) H \tag{A1}$$

such that $H(0) = H_0$ and $H(\tau) = H$. The time evolution operator associated with $H(t)$ is

$$U_\tau(t) = \mathcal{T} \exp\left[-i \int_0^t ds\, H(s\tau)\right] \tag{A2}$$

where $\mathcal{T}$ is the time ordering operator. In the limit of $\tau \to \infty$ the *adiabatic theorem* guarantees that, under general hypothesis [5, 6], the n-th eigenstate $|\omega_n\rangle$ of H_0 is evolved by thermalization evolution into

$$\lim_{\tau \to \infty} U_\tau(1) |\omega_n\rangle = |\Omega_n\rangle, \tag{A3}$$

where $|\Omega_n\rangle$ the n-th eigenstate of H. In the main text we use U_τ to refer to $U_\tau(1)$.

Appendix B: Ising SGS

Our aim is to find an initial state that will guarantee the SGS state as defined in Equation (1) when it undergoes the thermalization process, where we will be switching on the magnetic field h_z. To help us in this we introduce the following operator:

$$\mathcal{R} = \bigotimes_{j=0}^{L-1} R_z^j(\pi) \tag{B1}$$

where R_z^j is a rotation around the z-axis on the jth qubit. This operator commutes with the Hamiltonian for any value of J. This ensures the expectation value is conserved during the whole AT. It is worth noting that the auxiliary Hamiltonian ground states, $|+\rangle^{\otimes L}$ and $|-\rangle^{\otimes L}$, do not diagonalize since

$$\mathcal{R}|\pm\rangle^{\otimes L} = (-i)^L |\mp\rangle^{\otimes L} \tag{B2}$$

However, it is enough to consider the change of basis

$$|\Phi^\pm\rangle = \frac{1}{\sqrt{2}} \left(|+\rangle^{\otimes L} \pm |-\rangle^{\otimes L}\right) \tag{B3}$$

to have

$$\mathcal{R}|\Phi^\pm\rangle = \pm(-i)^L |\Phi^\pm\rangle. \tag{B4}$$

We now move our attention to the $|SGS\rangle$ state, that we want to obtain at the end of the AT, in the $h_3/J_1 \to \infty$ limit. In this regime the (non-degenerate) ground state is

$$|\Omega_0\rangle^{\otimes L} \equiv \bigotimes_j \frac{1}{\sqrt{2}} \left(|+\rangle + |-\rangle\right)_j \tag{B5}$$

and respects

$$\mathcal{R}|\Omega_0\rangle^{\otimes L} = (-i)^L |\Omega_0\rangle^{\otimes L}. \tag{B6}$$

The ground state $|0\rangle^{\otimes L}$ and $|\Phi^+\rangle$ share the same eigenvalue with respect to $\mathcal{R}$, which is preserved during the evolution. It is evident that

$$\lim_{\tau \to \infty} U_\tau |\Phi^+\rangle = |\Omega_0\rangle \tag{B7}$$

and, consequently,

$$\lim_{\tau \to \infty} U_\tau |\Phi^-\rangle = |\Omega_1\rangle. \tag{B8}$$

Moreover, if this is true for $h_3/J_1 \to \infty$ it is true for the cases of finite h_3/J_1, that require a shorter thermalization process. From Equations (B7) and (B8) we finally obtain

$$\lim_{\tau \to \infty} U_\tau |+\rangle^{\otimes L} = |SGS(0,1)\rangle. \tag{B9}$$

Appendix C: Observable choice

For the SGS procedure to work the objective is to have an observable O that maximizes ρ, as described in Equation (3). This facilitates a more straightforward estimation of the period of the cosine function, which in turn simplifies the fitting process for the energy gap.

Ising Model

For the Ising model our objective is to find an operator O that maximizes ρ independent of the chain/lattice size. A first set of numerical calculations shows that there are two operators that achieved this: either exactly 1 σ^3 (on any site) and the rest σ^0, or exactly 1 σ^1 (on any site) and the rest σ^2. This holds for all Ising chains with periodic boundary conditions up to 10 sites. Further numerical experiments show that these same observable maximize ρ for Ising lattices with up to 9 sites.

Then, we conjecture that the operators

$$O_1 = \sigma_j^3 (\sigma^0)^{\otimes L-1} \tag{C1}$$

and

$$O_2 = \sigma_j^1 (\sigma^2)^{\otimes L-1} \tag{C2}$$

maximize ρ as described in equation (3) for an arbitrary Ising chain/lattice with L-sites, where O_1 is a σ^3 on the jth site and the rest σ^0, and O_2 is a σ^1 on the jth site and the rest σ^2.

All our experiments involving the Ising model use the operator O_1 to estimate the energy gap. The choice of O_1 is due to the fact that it is simple to implement in the circuit.

Molecules

For small molecules the choice of operator is based on the following considerations. Since both ground and excited state of the auxiliary Hamiltonian are in the computational basis, it is always possible to find a tensor product, P, of identities and σ^1 Pauli matrices such that

$$\langle \omega_1 | P | \omega_0 \rangle = \langle \omega_1 | \bigotimes_{j=1}^{L} \sigma_j^{i_j} | \omega_0 \rangle = 1, \quad i_j \in \{0, 1\}. \tag{C3}$$

If the off diagonal terms of H are small with respect to the diagonal terms, then choosing P as the operator for the SGS procedure is unlikely to give $\rho = 0$. In particular

$$\rho = |\langle \Omega_1 | P | \Omega_0 \rangle| = |\langle \omega_1 | U_\tau^\dagger P U_\tau | \omega_0 \rangle| \tag{C4}$$

is unlikely to vanish. This is the operator choice for both H_2 and He_2 molecules.

Appendix D: Chebyshev nodes

The choice of the times used to fit $O(t)$ may be critical, in the case that they are uniformly distributed, because they could accidentally coincide with the nodes of the cosine function. If this was the case, no oscillation of $O(t)$ could be detected. Times are chosen as Chebyshev nodes [13] to avoid this possibility.

Appendix E: Intrinsic error estimation

Let

$$\langle O \rangle = \langle \psi | O | \psi \rangle \tag{E1}$$

be the expectation value of an operator O on a quantum state $|\psi\rangle$, and let

$$\langle (O - \langle O \rangle)^2 \rangle \tag{E2}$$

be its variance. Recalling that O should be unitary and Hermitian in order to be measured on a quantum computer

$$O^2 = O^\dagger O = \mathbb{1}, \tag{E3}$$

so that its eigenvalues can only be $\{+1, -1\}$. One can then decompose the state onto two eigenstates of O as

$$|\psi\rangle = \alpha|\psi_{+1}\rangle + \beta|\psi_{-1}\rangle \tag{E4}$$

with

$$\begin{cases} O|\psi_{\pm 1}\rangle = \pm|\psi_{\pm 1}\rangle \\ |\alpha|^2 + |\beta|^2 = 1. \end{cases} \tag{E5}$$

Then

$$\begin{cases} \langle O \rangle = |\alpha|^2 - |\beta|^2 \\ \langle (O - \langle O \rangle)^2 \rangle = 4|\alpha|^2|\beta|^2 \end{cases} \tag{E6}$$

Appendix F: More details on IonQ Aria

a. IonQ Native Gates

Since single qubit-gates are typically implemented on ion-trapped hardware with high average gate fidelity, potential issues in result's fidelity (when running a circuit on NISQ hardware) primarily stem from 2-qubit gates. For this reason, we simulate the Ising model with interactions along the x-axis and transverse field along the z-axis. This allows us to use only the native entangling gates available for IonQ Aria device, i.e. Mølmer-Sørensen gate [14], and to reduce the number of entangling gates only to the essential ones. More precisely, in a single Trotter step, one only needs two layers of entangling gates (see Figure 4), implying 80 2-qubit gates depth when fixing the number of steps to 40.

The Mølmer-Sørensen gate matrix is

$$\text{MS}(\phi_0, \phi_1, \theta) = \begin{pmatrix} \cos\frac{\theta}{2} & 0 & 0 & -ie^{-i(\phi_0+\phi_1)}\sin\frac{\theta}{2} \\ 0 & \cos\frac{\theta}{2} & -ie^{-i(\phi_0-\phi_1)}\sin\frac{\theta}{2} & 0 \\ 0 & -ie^{i(\phi_0-\phi_1)}\sin\frac{\theta}{2} & \cos\frac{\theta}{2} & 0 \\ -ie^{i(\phi_0+\phi_1)}\sin\frac{\theta}{2} & 0 & 0 & \cos\frac{\theta}{2} \end{pmatrix}. \qquad \text{(F1)}$$
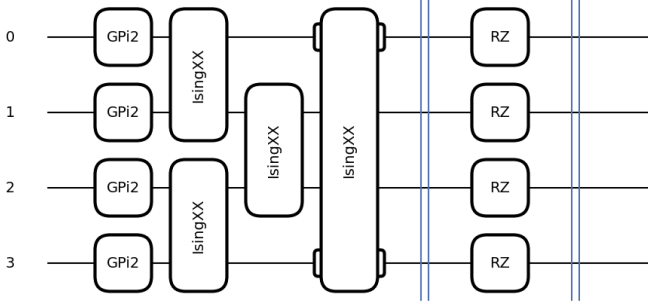

FIG. 4: Quantum circuit representation for a single Trotter step illustrating the evolution of the Spectral Gap Superposition (SGS) state. The circuit involves the application of GPI2(ϕ), RZ(θ), and IsingXX(θ) gates to prepare the SGS state for subsequent spectral gap estimation.

This gate matrix can be further simplified to obtain the Ising interaction $\sigma_i^1 \sigma_j^1$ by setting ϕ_0 and ϕ_1 equal to 0.

b. IonQ Aria noise model

To assess the resilience of our approach to noise, we incorporated a realistic noise model taking into account the technical features of IonQ's Aria device available online [15]. The noise sources considered include:

- *Thermal Relaxation*: This source of noise accounts for the effects of the thermal relaxation times T_1 and T_2. Notably, IonQ Aria has $T_1 = 100s$ and $T_2 = 1s$, and while we took them into account in our simulations, their effects were found to be negligible and did not significantly impact the results.

- *Gate Fidelity*: We simulated errors arising from finite gate fidelity, modeled as depolarizing noise. The relationship between gate fidelity and the depolarizing parameter is derived from what reported in the Appendix of [16]. The two-qubit gate time is $600\mu s$, while single qubit gates are executed in $135\mu s$.

- *Readout Noise* A readout noise of 0.39% was introduced to emulate imperfections in the measurement process.

Upon detailed examination, we have determined that the gate fidelity plays a significant role in the estimation of the spectral gap. This noise source has been implemented
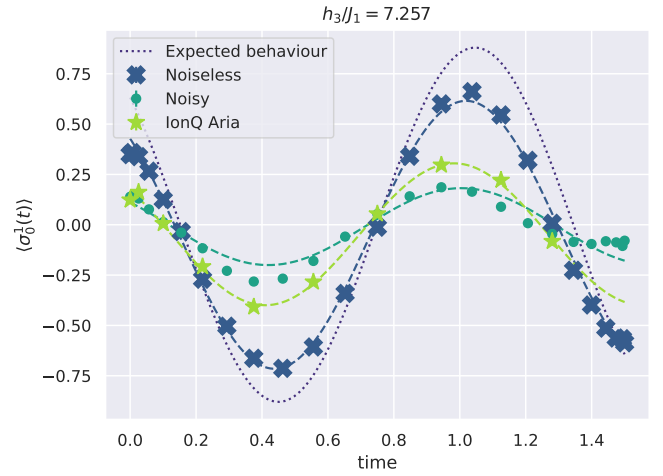

FIG. 5: Observable oscillations in time for Ising 1D chain with $L = 4$ at $h_3/J_1 = 7.257$, measured (points) and fitted (dashed lines) for noiseless, noisy and real hardware (with error mitigation). For reference, it is also reported the expected oscillatory from exact diagonalization (dotted line). Error bars represent a single standard deviation computed from the fit.

by considering a single qubit depolarizing channel, which acts on a density matrix Ψ

$$\mathcal{D}_p(\Psi) = (1-p)\Psi + p\frac{\mathbb{1}}{2}\Psi \ . \qquad \text{(F2)}$$

To take into account gate imperfections and finite qubit relaxation times we define the probability p as

$$p = 1 + 3\frac{2\epsilon - 1}{d} \ . \qquad \text{(F3)}$$

Here, $d = \exp\{-T_g/T_1\} + 2\exp\{-T_g/T_2\}$ and $\epsilon = 1 - F$, where F is the average gate fidelity. We define two depolarizing channels one per each type of gate (single/two-qubit gate).

Our approach demonstrates robustness against gate fidelity errors and readout noise, suggesting its viability for simulation on real quantum hardware.

The noise resilience analysis results are presented in Figure 2. The robustness of our approach can be appreciated also in the time oscillations of the observable reported in Figure 5. There it is highlighted how oscillations are damped by the noise (reduced ρ) with respect to the expected behaviour $\rho\cos(\Delta E + \theta)$. For the expected behaviour we employ ρ given by our preliminary
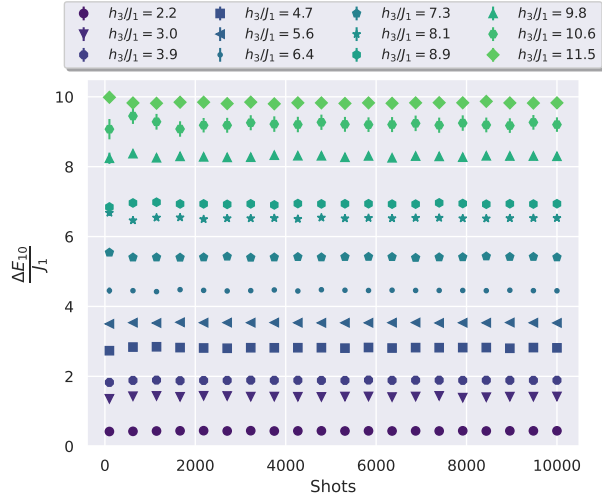
FIG. 6: Robustness testing over increasing number of shots. Scatter points correspond to measured value of the spectral gap in J_1 units. Error bars represent a single standard deviation computed from the fit.

study on the value of the observable and we set the same phase θ as the noiseless simulations. Interestingly the noise mitigation allows for having wider oscillations on real hardware compared to noisy simulations.

In particular, the IonQ Aria device reduces the impact of systematic errors by employing a specific error mitigation method called *debiasing* [17]. This technique maps a circuit into multiple variants, employing different qubit permutations or gate decompositions.

The effectiveness of debiasing error mitigation is likely improved by our approach's robustness to a reduced number of shots. In fact, as reported in Figure 6, we assess the robustness of our approach over a reduced number of shots by reducing this value up to 100 shots. As witnessed by Figure 6, the spectral gap estimate stays approximately constant over the different number of shots.

Appendix G: Ising Lattice experiments

Here we present further experiments related to an Ising lattice with 4 sites and periodic boundary conditions (see Figure 7). All previous conditions for the Ising chain experiment remain in this study. In particular, the 40 Trotter steps are divided in 15 thermalization steps and 25 time evolution steps. In the 2D simulations, the number of entangling gates required per Trotter step is doubled with respect to the 1D model. Due to the prohibitive depth implied by the extra interactions, simulations with real hardware noise model lead to inconclusive results. It would be interesting to see if IonQ Aria noise mitigation is able to lead to measurable results.

[1] M. Troyer and U.-J. Wiese, Computational complexity and fundamental limitations to fermionic quantum monte carlo simulations, Physical review letters **94**, 170201 (2005).

[2] J. Preskill, Quantum Computing in the NISQ era and beyond, Quantum **2**, 79 (2018).

[3] J. M. Leamer, A. B. Magann, A. D. Baczewski, G. Mc-Caul, and D. I. Bondar, Spectral gaps via imaginary time (2023), arXiv:2303.02124 [quant-ph].

[4] A. E. Russo, K. M. Rudinger, B. C. A. Morrison, and A. D. Baczewski, Evaluating energy differences on a quantum computer with robust phase estimation, Phys. Rev. Lett. **126**, 210501 (2021).

[5] M. Born and V. Fock, Beweis des adiabatensatzes, Zeitschrift für Physik **51**, 165 (1928).

[6] S. Jansen, M.-B. Ruskai, and R. Seiler, Bounds for the adiabatic approximation with applications to quantum computation, Journal of Mathematical Physics **48**, 102111 (2007).

[7] H. F. Trotter, On the product of semi-groups of operators, Proceedings of the American Mathematical Society **10**, 545 (1959).

[8] K. Huang, *Statistical mechanics* (John Wiley & Sons, 2008).

[9] G. Rendon, J. Watkins, and N. Wiebe, Improved Accuracy for Trotter Simulations Using Chebyshev Interpolation, Quantum **8**, 1266 (2024).

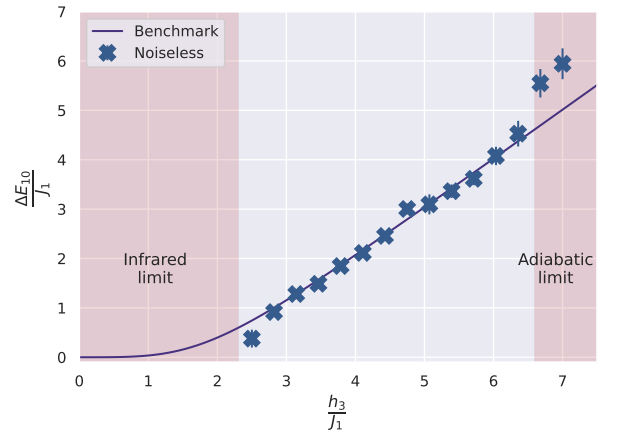[10] N. Moll, A. Fuhrer, P. Staar, and I. Tavernelli, Optimizing qubit resources for quantum chemistry simulations

FIG. 7: Spectral gap as a function of h_3/J_1 for a $L = 4$ Ising 2D lattice with periodic boundary conditions (PBC). Our approach demonstrates optimal agreement with the benchmark values, in the noiseless case. Error bars represent a single standard deviation computed from the fit.

in second quantization on a quantum computer, Journal of Physics A: Mathematical and Theoretical **49**, 295301

(2016).

[11] R. Shankar, *Quantum field theory and condensed matter: An introduction* (Cambridge University Press, 2017).

[12] K. Gnatenko, H. Laba, and V. Tkachuk, Energy levels estimation on a quantum computer by evolution of a physical quantity, Physics Letters A **424**, 127843 (2022).

[13] P. L. Chebyshev, *Théorie des mécanismes connus sous le nom de parallélogrammes* (Imprimerie de l'Académie impériale des sciences, 1853).

[14] A. Sørensen and K. Mølmer, Quantum computation with ions in thermal motion, Physical review letters **82**, 1971 (1999).

[15] IonQ, Ionq aria: practical performance (2024).

[16] C. Blank, D. K. Park, J.-K. K. Rhee, and F. Petruccione, Quantum classifier with tailored quantum kernel, npj Quantum Information **6**, 41 (2020).

[17] A. Maksymov, J. Nguyen, Y. Nam, and I. Markov, Enhancing quantum computer performance via symmetrization, arXiv preprint arXiv:2301.07233 https://doi.org/10.48550/arXiv.2301.07233 (2023).